Adaptive Force Tracking Control of a Magnetically Navigated Microrobot in Uncertain Environment

Xiaodong Zhang and Mir Behrad Khamesee, *Member, IEEE*

***Abstract*—Magnetic navigation microrobotics is a promising technology in micromanipulation and medical applications. A magnetically navigated microrobot (MNM) usually has permanent magnets or ferromagnetic materials attached to it to create interaction force for navigation in the presence of an external magnetic field. During the exploration of the MNM, it is necessary to simultaneously control the position of the MNM and the contact force when the microrobot is constrained by its environment. However, owing to the small size of an MNM and noncontact property of magnetic levitation, installing on-board force sensors is very challenging. This paper presents a dual-axial interaction force determination mechanism that uses magnetic flux measurement, with no need for a conventional on-board force sensor. The interaction force is then used as the feedback force of a position-based impedance controller to actively track the reference force on the MNM in uncertain environment. To reduce the force tracking error caused by environmental uncertainty, an adaptive control algorithm is implemented to generate a reference motion trajectory that attempts to minimize the force error to an acceptable level. The force tracking performance of the robot is experimentally validated. A 2.01 μN root mean square force tracking error is reported. The proposed technique can be applied to biomedical microsurgery, such as for cutting tissue with controlled force.**

***Index Terms*—Adaptive force tracking, magnetic navigation, microrobotics, microsurgery, off-board force.**

I. Introduction

FORCE control is important to robust and dexterous manipulation when a manipulator works in a constrained environment. Manipulators with force control capability have been implemented for macro- and micromanipulation tasks, such as surgical assistance [1], painting [2], peg-in-hole operations [3], cell injection [4], and microsurgery [5]. With force control,the simultaneous protection of the manipulator and its environment is achieved.

Many researchers have studied force control of manipulators by implementing various controller algorithms. Generally, these algorithms are categorized into hybrid position/force control [6], [7] and impedance control [8]. Within the impedance control framework, a desired second-order model is assigned to a manipulator. The desired model enforces a relation between the position error dynamic and the force tracking error. A steady-state zero force error is obtainable if the reference position trajectory of the impedance controller is well designed. Generally, the reference position trajectory can be designed based on known environmental parameters, i.e., the nontouched state position and the stiffness of the environment. However, in real applications, the environment is not known or only partially known. Therefore, a perfect reference position trajectory is not always obtainable, leading to steady-state force tracking errors. Numerous attempts to deal with environmental uncertainty in force tracking have been reported in the literature [9]–[11], [28]. In [12], an adaptive impedance controller was proposed to solve the force tracking problem when a manipulator is in contact with an unknown environment. Zero manipulator stiffness was used to realize the steady-state zero force tracking error, while the adaptive law utilized the force tracking error to update the impedance parameter of the desired impedance model. Seraji and Colbaugh [13] proposed direct and indirect adaptive impedance controllers for force tracking in an uncertain environment. For the direct controller, model reference adaptive control law was applied to update the reference trajectory of the impedance controller. For the indirect controller, the reference motion trajectory was calculated after estimating the environment stiffness and position, both updated based on force tracking error. Advanced control methods, such as neural networks, were also applied to improve the force tracking performance of manipulators in an uncertain environment [14], but this type of controller requires a huge amount of training data, which is not always easy to collect. The research in the literature was conducted only on manipulators that had a mechanical joint. The adaptive force tracking issue has not been studied for magnetically navigated manipulators.

Magnetically navigated microrobotics is an emerging technique that uses magnetic energy to remotely guide a microrobot. Thanks to its dust-free and contactless manipulation features, the magnetically navigated microrobot (MNM) has a promising potential in biomedical applications, such as invasive microsurgery

Manuscript received June 3, 2016; revised September 28, 2016, December 13, 2016, and March 13, 2017; accepted May 9, 2017. Date of publication May 26, 2017; date of current version August 14, 2017. Recommended by Technical Editor Y. Tian. This work was supported in part by the Canada Foundation for Innovation, and in part by the Natural Science and Engineering Research Council of Canada. *(Corresponding author: Mir Behrad Khamesee.)*

The authors are with the Department of Mechanical and Mechatronics Engineering, University of Waterloo, Waterloo, ON N2L 3G1, Canada (e-mail: x442zhan@uwaterloo.ca; khamesee@uwaterloo.ca).

Color versions of one or more of the figures in this paper are available online at http://ieeexplore.ieee.org.

Digital Object Identifier 10.1109/TMECH.2017.2705523

and drug delivery. Several magnetic navigation prototypes have been developed for future implementation in biomedical applications [15]–[19]. However, the published research concentrates merely on the precise positioning of MNMs. The contact force on the microrobot was not considered, which would result in failure of levitation or damage the structures that the microrobot works with.

In this paper, we propose using a position-based impedance control mechanism to actively track the reference force when an MNM is in contact with its environment. Since the active force regulation requires force feedback from a force sensor, a dual-axial off-board force determination method is introduced to overcome the common limitation of installing a force sensor on a tiny levitated microrobot [20]. In addition, the force tracking problem is solved by adopting an adaptive law that ensures asymptotic stability. The reference position trajectory is calculated from the estimated stiffness and the position of the contact surface. The experimental results are presented to show the adaptive force tracking performance of the levitated microrobot. The technique proposed has great potential for application in biomedical microsurgery. The main contribution of this paper involves design and implementation of an adaptive force tracking controller to regulate the contact force between an MNM and its uncertain environment, which has never been considered in existing literature.

This paper is organized as follows. Section II briefly introduces the magnetic navigation system and the microrobot dynamics. The position-based impedance control and adaptive environmental parameters estimation algorithms are presented in Section III. Section IV explains the dual-axial off-board force prediction mechanism that uses magnetic flux measurement. The experimental validation of the proposed force tracking technique is shown in Section V. Conclusions are given in Section VI.

II. Magnetic Navigation

A. System Description

A magnetic navigation system was previously developed in the Maglev lab at the University of Waterloo. The system, as shown in Fig. 1, consists of a magnetic drive unit with six pairs of electromagnets, an iron yoke that forms the magnetic circuit and enhances the magnetic field strength in the workspace, a microrobot with a permanent magnet core, and three sets of laser beam sensors installed to detect the three-dimensional position of the navigated microrobot.

B. Principle of Levitation

Magnetic levitation results from the interaction between a magnetic field and a magnetized object. While the system is levitating the object, the system produces a uniform magnetic field in the workspace. The magnetic field has only one minimum magnetic potential energy point which is defined as $B_{\max}$ [15]. In free levitation, the location of $B_{\max}$ is the location of the object. The translation of the object is realized by changing the location of the $B_{\max}$ point. In order to levitate a magnetized object, the levitation force should be enough to compensate for

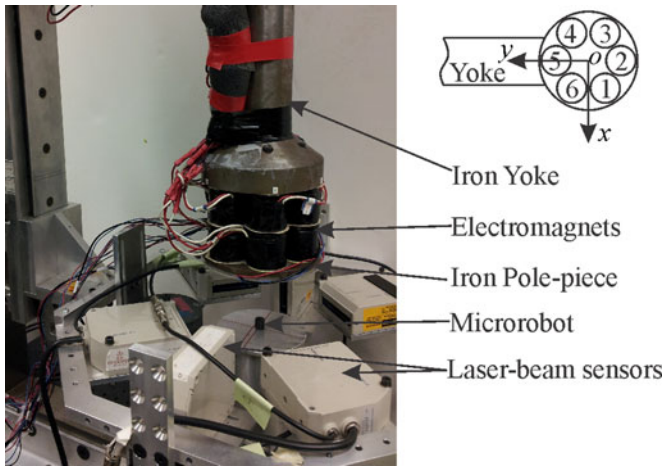

Fig. 1. Magnetic navigation system developed at the University of Waterloo.

the gravity force of the object. When a unit volume permanent magnet with internal magnetization M is placed in an external magnetic field with magnetic flux density B, the interaction force can be calculated as $F = \nabla (M \cdot B)$. ∇ indicates the gradient of a vector. If a permanent magnet with volume V is uniformly magnetized in one direction $M = [0,\ 0,\ M_z]$, the force is simplified as $F = M_z V(\nabla\ B_z)$. The force model is used for analyzing the translational dynamics of the permanent magnet. While there is misalignment between the magnetization direction of the permanent and the external magnetic field, the rotational motion also occurs. In that case, the magnetic torque on the permanent magnet is which aligns the magnetization direction to the external magnetic field direction.

C. Dynamics of the Magnetically Navigated Microrobot

Based on our previous study on the same magnetic levitation system, the dynamic models of a levitated permanent in three translational directions are expressed as [20]

$$m\ddot{x} = 3x(a_x + a_y)I_0 + b_x \underbrace{(i_1 - i_3 - i_4 + i_6)}_{u_x} + F_{e,x} \tag{1}$$

$$m\ddot{y} = 3y(a_x + a_y)I_0 + b_y \underbrace{(i_1 + 2i_2 + i_3 - i_4 - 2i_5 - i_6)}_{u_y} + F_{e,y} \tag{2}$$

$$m\ddot{z} = a_z I_0 z + (a_z z_0 + b_z) \underbrace{(i_1 + i_2 + i_3 + i_4 + i_5 + i_6)}_{u_z} + F_{e,z} \tag{3}$$

where m is the mass of the microrobot, and x, y, and z are real three-dimensional positions of the microrobot in the workspace. I_0 is the current in all electromagnets while the microrobot is levitated at the center of the workspace. The parameters a_x, a_y, a_z, b_x, b_y, b_z are evaluated from experimental measurements, while i_j $(j = 1, \ldots, 6)$ are the perturbed current of the jth electromagnet shown in Fig. 1. F_{ex}, F_{ey}, F_{ez} are the three-dimensional contact force exerted by environment. Since designing a

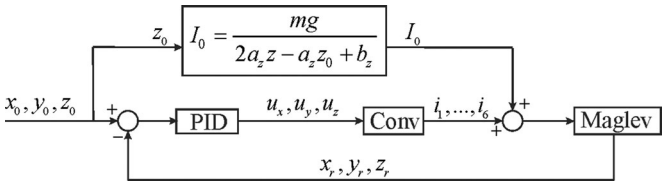

Fig. 2. PID plus feed-forward motion tracking controller for the magnetic navigation system.

controller that has six outputs is much more complex than a controller with only three outputs, three virtual inputs u_x, u_y, u_z are assigned for three-dimensional translational motion control of a feed-forward plus proportional-integral-derivative (PID) controller. The feed-forward controller provides the fundamental levitation current, while the PID controller regulates the perturbation caused by disturbance. The transformation from three virtual inputs to six current inputs using pseudo-inverse guarantees the least energy consumption. The position controller schematic is shown in Fig. 2. The motion controller provides 10 μm positioning accuracy in a 30 $\times$ 30 $\times$ 30 mm^3 working space [21].

III. Position-Based Impedance Control and Problem Formulation

In the majority of the literature, research has been conducted on force-based impedance control of manipulators by introducing an outer torque feedback loop at the joint space. This methodology is appropriate for manipulators with torque-controlled electrical actuators at joints. However, most commercialized robots emphasize the accuracy of position trajectory following, and do not provide a force control mode. Therefore, force-based impedance control was impossible on these manipulators. Alternatively, position-based impedance control is proposed to achieve compliant interaction of position-controlled manipulators [22], [23]. It is a position controller with set points regulated by a force feedback loop. The position-based impedance control is simple in that no robot dynamics are required. It only requires the controlled manipulator to have an accurate position tracking capability.

The magnetically levitated microrobot studied in this paper is position controlled by a PID plus feed-forward controller as presented in the above-mentioned section. It is assumed that the microrobot closely tracks the desired position trajectory. To track a force trajectory, the desired position command to the manipulator's position controller should be obtained from a target impedance controller that relates position error to force tracking error. The generalized target impedance controller is [24], [25]

$$M_d(\dot{Y}_r - \ddot{Y}_d) + B_d(\dot{Y}_r - \dot{Y}_d) + K_d(Y_r - Y_d) = K_f(F - F_r) \tag{4}$$

where M_d, B_d, K_d, K_f are positive definite inertial, damping, stiffness, and force parameters of the target impedance model; Y_r and Y_d indicate the reference and actual trajectory of the micromanipulator end-effecter; F_r is the reference contact force that the microrobot tracks; and F represents the actual contact force applied to the environment by the microrobot.

Within the target impedance model, the desired position trajectory can be calculated as

$$Y_d = Y_r + K_d^{-1}\{M_d(\ddot{Y}_r - \ddot{Y}_d) + B_d(\dot{Y}_r - \dot{Y}_d) - K_f(F - F_r)\} \tag{5}$$

which is a function of reference position, reference force, and actual force. In a free levitation situation, the reference and real contact force are chosen as zero. Then, the impedance model is a pure position controller. Otherwise, the reference position should be carefully chosen in order to track the reference force.

In real applications, the actual force can be obtained from the parameters of environment

$$F = K_e(Y - Y_e) \tag{6}$$

where K_e and Y_e are, respectively, the stiffness and original location of environment, Y is the actual position of the microrobot, and $Y = Y_d$ if the microrobot has accurate position tracking capability. Let $E_\mathrm{f} = F_\mathrm{r} - F$ denotes the force tracking error. The actual microrobot position can be expressed as

$$Y = Y_e + K_e^{-1}F = Y_e + K_e^{-1}(F_r - E_f). \tag{7}$$

Substituting (7) into (4), the following steady-state force tracking error expression is obtained

$$E_f = (K_d K_e{}^{-1} + K_f)^{-1}\{K_d K_e{}^{-1} F_r + K_d(Y_e - Y_r)\}. \tag{8}$$

From (8), in order to closely track the reference force trajectory, the reference position trajectory should be selected as

$$Y_r = Y_e + K_e^{-1}F_r. \tag{9}$$

However, in reality, the values K_e and Y_e of environment are not always known precisely. Therefore, an adaptive law is presented in the following section to compensate for parameter uncertainty.

IV. Adaptive Force Tracking in Uncertain Environment

Let $x_r, x_d, x_e, k_e, k, f_r, f$ be the elements of $Y_r, Y_d, Y_e, K_e, F_r, F$. Here, only one-dimensional situation is considered. Multidimension force tracking can be achieved in the same way.

Let $\hat{k}_e$ and $\hat{x}_e$ be the estimation of k_e and x_e, respectively. Replacing with the estimated value in (7) and (9), one gets

$$x = \hat{x}_e + \frac{f}{\hat{k}_e} = \hat{x}_e + \frac{1}{\hat{k}_e}(f_r - e_f) \tag{10}$$

$$x_r = \hat{x}_e + \frac{f_r}{\hat{k}_e}. \tag{11}$$

Then, the error between reference input and actual position is

$$x_r - x = \frac{e_f}{\hat{k}_e}. \tag{12}$$

Substituting the error expression into the impedance dynamic model (4), the force tracking error dynamic model is obtained as

$$m_d\ddot{e}_f + b_d\dot{e}_f + (k_d + \hat{k}_e k_f)e_f = 0 \tag{13}$$

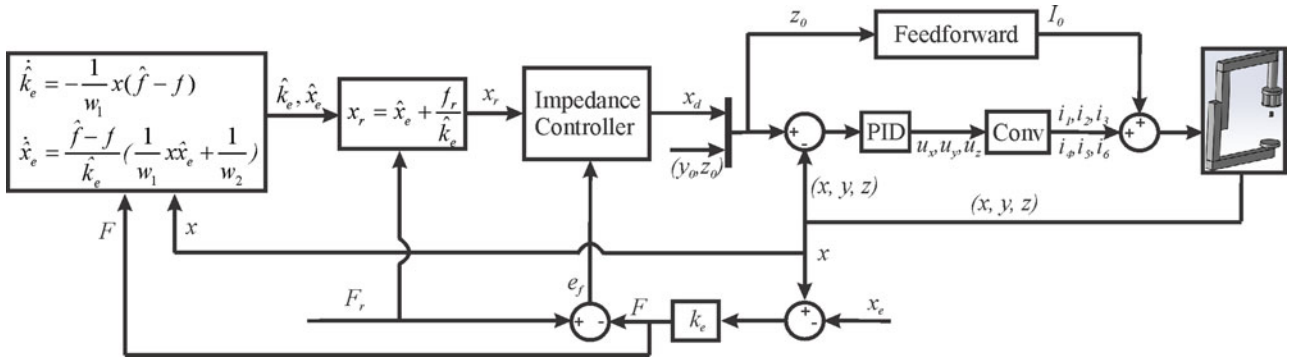

Fig. 3. Force tracking control system schematic with adaptive environmental parameters estimation and impedance control.

where m_d, b_d, k_d, k_f are elements of M_d, B_d, K_d, K_f. It shows that (13) is asymptotically stable if all its parameters are positive definite. The force tracking error convergences to zero as time goes to infinite.

Letting $\hat{f} = \hat{k}_e(x - \hat{x}_e)$ be the estimated contact force using estimated parameters allows the estimated parameters $\hat{k}_e$ and $\hat{y}_e$ to be updated such that the estimated force converges to real contact force f. The level of convergence is denoted using the error expression between estimated force and real force

$$\hat{f} - f = \hat{k}_e(x - \hat{x}_e) - k_e(x - x_e) = (\hat{k}_e - k_e)x + (k_e x_e - \hat{k}_e \hat{x}_e). \quad (14)$$

Defining $\tilde{k}_e = \hat{k}_e - k_e$ as the estimation error of environment stiffness, the convergence of estimated values to real values is guaranteed if the parameters estimation error converges to zero as time elapses.

Consider the following Lyapunov function candidate:

$$V = \tilde{k}_e^T w_1 \tilde{k}_e + (k_e x_e - \hat{k}_e \hat{x}_e)^T w_2 (k_e x_e - \hat{k}_e \hat{x}_e) \quad (15)$$

where w_1 and w_2 are constant positive numbers that make V nonnegative. As presented in [13], if the estimations of $\hat{k}_e$ and $\hat{x}_e$ are updated using the following algorithm, the estimation values will finally converge to the real value of environmental parameters:

$$\dot{\hat{k}}_e = -\frac{1}{w_1} x \left(\hat{f} - f\right) \quad (16)$$

$$\dot{\hat{x}}_e = \frac{\hat{f} - f}{\hat{k}_e} \left(\frac{1}{w_1} x \hat{x}_e + \frac{1}{w_2}\right). \quad (17)$$

Then, the time derivative of V is expressed as

$$\dot{V} = 2\tilde{k}_e^T w_1 \dot{\hat{k}}_e - 2(\hat{k}_e \hat{x}_e - k_e x_e)^T w_2 (\dot{\hat{k}}_e \hat{x}_e + \hat{k}_e \dot{\hat{x}}_e). \quad (18)$$

The constant property of k_e, x_e is used when deriving the derivative of the Lyapunov function. Substituting (16) and (17) into (18), and simplifying by some algebraic operation, we can reduce (18) to

$$\dot{V} = -2(\hat{f} - f)^2 \quad (19)$$

which is negative semidefinite. Equations (15) and (19) indicate that, if update laws (16) and (17) are applied, the estimation parameters converge to their real values as evolution continues. This implies that the reference force is tracked, since (9) and (11) indicate an optimal trajectory is generated using the estimated values. The resultant adaptive controller schematic is presented in Fig. 3.

V. Dual-Axial Off-Board Force Determination

The adaptive control law presented above requires the real-time force feedback, which is conventionally obtained by installing a force sensor at the end-effecter of a manipulator. However, the magnetically navigated micromanipulator is remotely manipulated without any mechanical connection between the end-effecter and the manipulator base. Therefore, it is not practical to install an on-board force sensor. In addition, attaching a force sensor on the end-effecter can significantly increase MNM's total mass and energy consumption of the system. In order to solve these limitations, we propose using the off-board force determine mechanism to predict the real-time contact force on the navigated micromanipulator. The technique was first successfully reported on one-dimensional force determination [26]. As part of the novel contributions of this paper, the two-dimensional force determination mechanism which can be implemented in unknown environment is presented.

In the steady-state of a free levitation, the MNM stays at the minimum magnetic potential energy point in a horizontal plane. See Fig. 4(a). This minimum magnetic potential energy point is the location of the maximum magnetic flux density ($B_{\max}$) point where zero horizontal magnetic field gradient is guaranteed [15]. However, when the microrobot is in contact with environment, the magnetic field applies force to pull the microrobot toward a reference position. In this situation, the steady-state horizontal position of the microrobot is different from the $B_{\max}$ point, since a nonzero gradient is required at the stabilized position in order to produce sufficient force. The concept is presented in Fig. 4(b). The magnetic force is related to the distance between the $B_{\max}$ location/point and the real position of the microrobot. For two-dimensional condition, the horizontal forces are expressed as

$$F_x = C_{x1} dx + C_{x2} x_{\max} y_{\max} dy \quad (20)$$

$$F_y = C_{y1} x_{\max} y_{\max} dx + (C_{y2} + 4x) dy \quad (21)$$

where (x, y) is the real position of the microrobot relative to the work coordinate system shown in Fig. 1. The real position is measured using laser beam sensors.dx and dy are the distance between $B_{\max}$ point and real position of the micro-

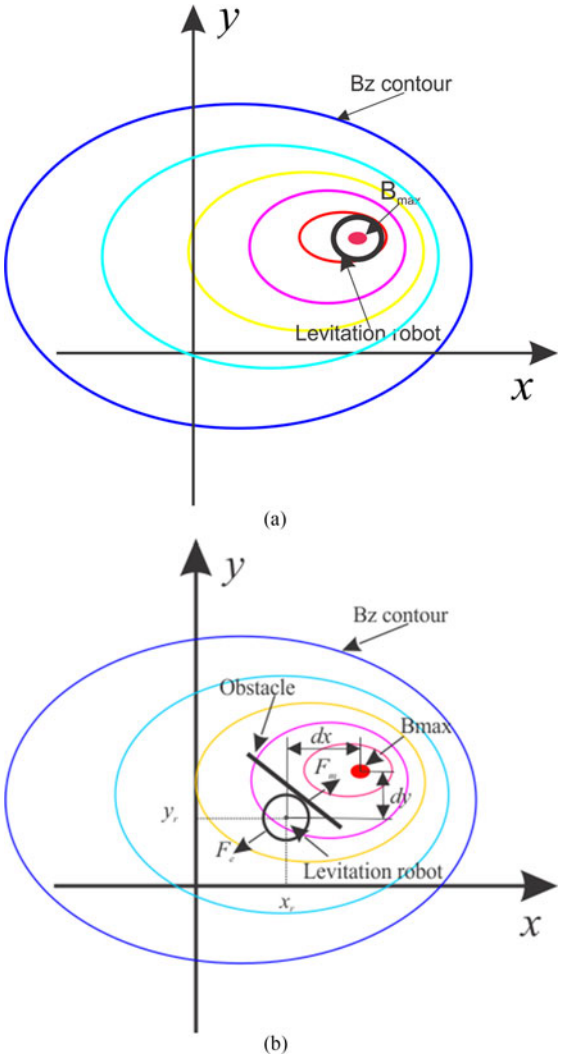

Fig. 4. Principle of magnetic navigation and off-board force determination using the concept of $B_{\max}$ point. (a) Free levitation. (b) Contact with environment.

robot. $C_{x1}, C_{x2}, C_{y1}, C_{y2}$ are constant coefficients that can be obtained from experiment, and $(x_{\max}, y_{\max})$ is the position of the $B_{\max}$ point. In our previous work [27], a technique for determining the dual-axial position of the $B_{\max}$ point in a horizontal plane was proposed. The idea is that the $B_{\max}$ point is determined by measuring the magnetic field pattern inside the working space. Four Hall-effect sensors are attached to the bottom of the iron pole-piece to measure the magnetic flux pass through the working space. Hall-effect sensors outputs are then used to map the magnetic field pattern in the working space. The installation of Hall-effect sensors is shown in Fig. 5. The install location of Hall-effect sensors requires obtaining a linear mapping between sensors output and microrobot position.

Off-board force determination in y-direction using similar mechanism was reported in [26]. The accuracy of force determination reported in the previous work was 1.27 μN. In the current paper, the force determination mechanism is validated in the x-direction, which is the main work direction of this research. Fig. 6 shows the force measurement using a cantilever beam and magnetic flux measurement in x-direction. It shows

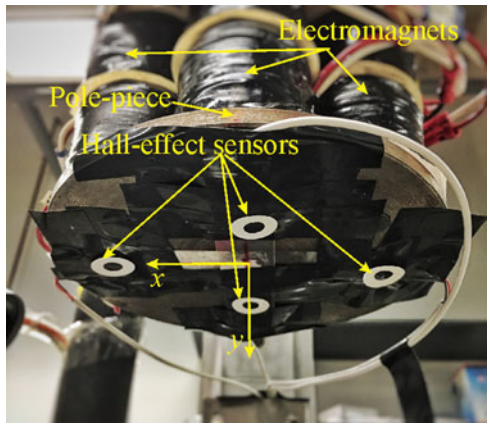

Fig. 5. Installation of four Hall-effect sensors at the bottom of the iron pole-piece.

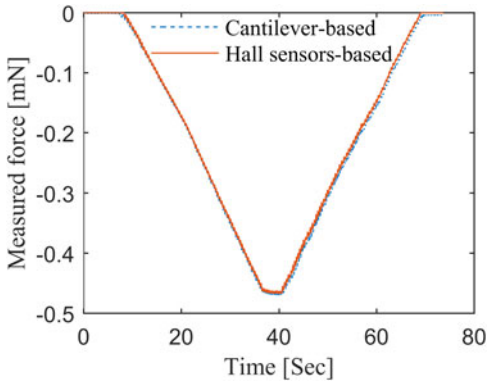

Fig. 6. Validation of force measurement accuracy using Hall-effect sensors in x-direction.

that the force determination using magnetic flux measurement provides 0.54 μN root mean square error.

VI. Experimental Validation

In this section, the force tracking performance of the MNM using the proposed algorithm is validated experimentally. For the purpose of showing the concept, only one-dimensional force tracking is studied in this paper. Specifically, we study the force tracking in x-direction relative to the coordinate system shown in Fig. 1.

In order to implement the proposed impedance algorithm and adaptive parameter estimation law on to a digital controller, (5), (16), and (17) are discretized. In this study, the sampling rate was set as 1 ms.

To demonstrate the performance of the proposed controller, experiments were conducted using the magnetic levitation microrobotics system. The control mechanism was compiled to run on a dSPACE DS1006 controller board. The controller processes the input signal from laser-beam sensors and Hall-effect sensors, and outputs a driving current signal to command the output current of an amplifier. A host computer functions as the human–machine interface to facilitate monitoring the real-time situation of the magnetically navigated robot.

The first experiment was conducted to validate the force tracking ability of the robot. The microrobot is a cylinder permanent

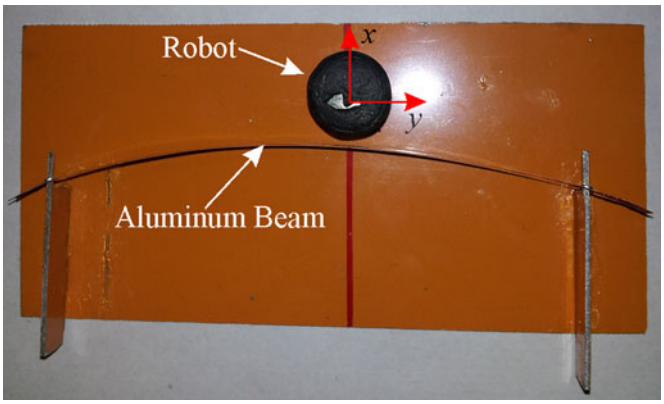

Fig. 7. Experimental setup for force tracking validation, the two ends of the bended aluminum beam are not fixed.

magnet with 10 mm in diameter, 10 mm in height, and 10.86 g in weight. The permanent magnet has 1.29 T remnant magnetic flux density. In this experiment, the microrobot was commanded to push a beam constrained at its two ends (see Fig. 7). The beam was a bended thin 6061 aluminum alloy sheet with 50 mm in length, 0.051 mm in thickness, and 3 mm in width. The exact location and stiffness of the beam are unknown. The experiment was conducted while the microrobot was levitated at 79 mm below the iron pole-piece. The force tracking performance was validated in the x-direction on the horizontal plane. While in the y-direction, position tracking accuracy is guaranteed. The parameters of the x-direction impedance controller were chosen as $m_d = 1$, $b_d = 10$, $k_d = 1.2$, $k_f = 1$. The impedance parameters were chosen to satisfy an over-damped levitation that improved the robustness of navigation. The parameters for the adaptive control law were $w_1 = w_2 = 1$. The initial values of parameter estimation were $k_e = 0.2\,\text{N/m}$, $x_e = -0.001\,\text{m}$.

The experimental result is shown Fig. 8. The experiment was divided into four phases. In the first phase, a very small reference contact force $F_r = 0.01$ mN was assigned to the impedance controller. The purpose of the small reference force was to maintain an initial contact between the navigated microrobot and the unknown surface. In the second phase, a ramp-type reference force trajectory was assigned for the microrobot to track. In the third phase, the robot was command to move in y-direction, while the maximum commanded contact force was maintained in x-direction. Meanwhile, the controller adjusted the desired x position. In the fourth phase, another ramp-type reference force trajectory was assigned for the microrobot to track until the initial 0.01 mN contact force was obtained again. This experiment demonstrates that the proposed algorithm exhibits good force tracking in the presence of environmental uncertainty. In Fig. 8(a), the accuracy of force tracking is 2.01 μN root mean square error. However, it should be noted that there was vibration while the reference force was 0.01 mN. This was because the force was too light to stabilize the beam. In Fig. 8(b), the estimated reference x position is obtained from adaptive estimator expressed in (10) and (11). The calculated desired x position is obtained from the position-based impedance controller expressed in (5). The update of estimated environment stiffness $\hat{k}_e$ is presented in Fig. 8(d). In order to clearly show the described procedure, real pictures while the microrobot was working are shown in Fig. 9.

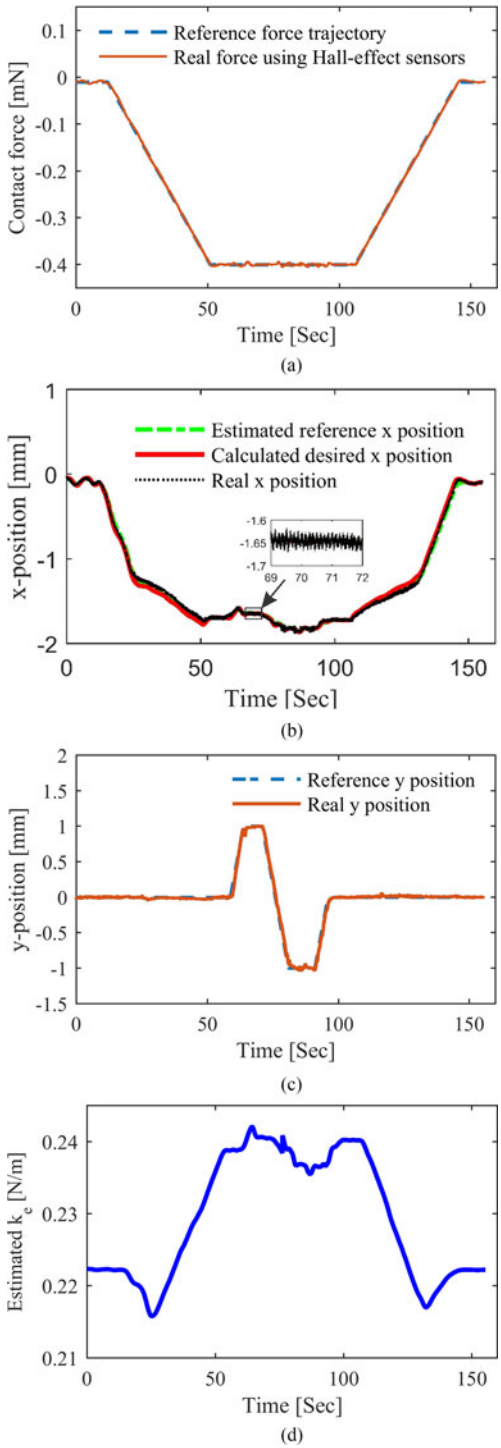

Fig. 8. Ramp force trajectory tracking performance of the magnetically navigated microrobot. (a) Force tracking Performance. (b) Position tracking in the x-direction. (c) Position tracking in the y-direction. (d) Estimated k_e in the process. (e) Magnetic levitation.

The performance of the controller is related to the parameters of adaptive control law and impedance controller. A desired performance can be achieved by carefully tuning these parameters. Fig. 10 shows the effect of the desired impedance damping coefficient on the response speed and overshoot in step force trajectory tracking. Fig. 10(a) shows the step response with relative small damping $b_d = 5\,\text{N}\cdot\text{s/m}$. By comparing with the

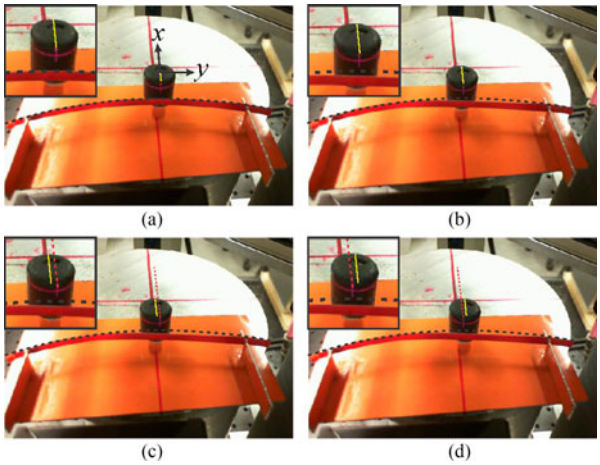

Fig. 9. Navigated microrobot pushing an Aluminum beam with controlled contact force in *x*-direction. (a) The microrobot started pushing with 0.01 mN force. (b) The contact force was set as 0.4 mN. (c) The microrobot moved to $y = 1$ mm while contact force in *x*-direction was kept as 0.4 mN. (d) The microrobot moved to $y = -1$ mm while contact force in *x*-direction was kept as 0.4 mN. For comparison, the reference curvature is shown in dotted line.

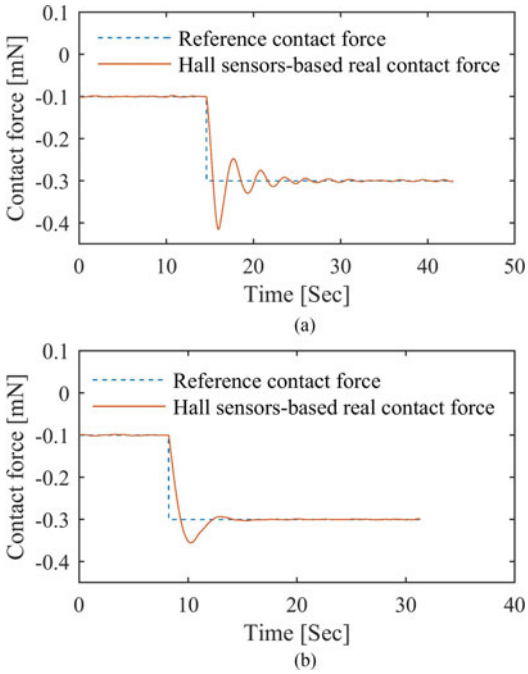

Fig. 10. Step response of force tracking with different impedance control damping: (a) $b_d = 5\,\mathrm{N}\cdot\mathrm{s/m}$; and (b) $b_d = 20\,\mathrm{N}\cdot\mathrm{s/m}$.

step response with larger damping $b_d = 20\,\mathrm{N}\cdot\mathrm{s/m}$ in Fig. 10(b), it shows that small damping results in more overshoot, longer stability time, and more oscillation. The presented technique can be applied to biomedical microsurgery using an MNM. One of the applications is using the microrobot with a very thin blade attached on it to cut delicate tissues. This is a process that does not require a large force compared to 0.5 mN.

To show the adaptive force tracking performance of the MNM in multi-axis, a second experiment which considered the step response of force tracking in the *y*-direction was conducted. In this experiment, the MNM was navigated to push the same aluminum beam in the first experiment. To start, a small reference force 0.01 mN guaranteed the initial contact between the MNM and the beam. Then, the MNM was commanded to track the step force trajectory. The parameters of the impedance controller in this experiment were set as $m_d = 1\,\mathrm{N}\cdot\mathrm{s}^2/\mathrm{m}$, $b_d = 20\,\mathrm{N}\cdot\mathrm{s/m}$, $k_d = 1.2\,\mathrm{N/m}$, $k_f = 40$. The experiments results are presented in Fig. 11. Fig. 11(a) shows the force tracking performance. It shows that the adaptive controller provides 1.63 μN force tracking error in steady state. Fig. 11(b) shows the motion trajectory of the MNM in the *y*-direction. The estimated reference *y* position is obtained from the position estimator in (11). The calculated desired *y* position is obtained from the position-based impedance controller. The real *y* position is obtained from laser-beam sensor.

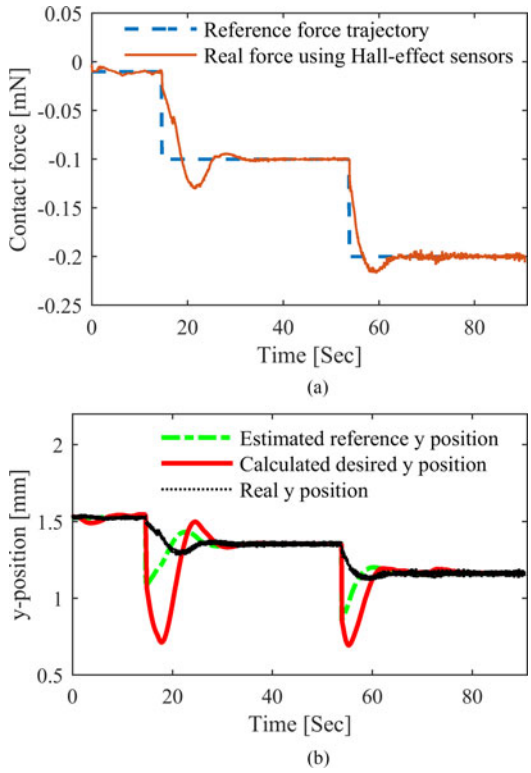

Fig. 11. Step response of adaptive force tracking in *y*-direction: (a) force tracking performance; and (b) position trajectories of the MNM in the *y*-direction. In (b), the calculated desired *y* position from the position-based impedance controller has relative large overshoot. This is because a small k_d was chosen in (5) for force tracking.

VII. Conclusion

A novel adaptive force tracking algorithm was presented in this paper that actively controls the contact force between an MNM and its environment. The stiffness and location of its environment are not necessarily known. In order to realize real-time force feedback, an off-board force determination mechanism was proposed in lieu of using an on-board force sensor. A ramp force trajectory tracking experiment was conducted to show the performance of the control system. Experimental results proved that the controller can achieve very good force tracking when the environment is uncertain. The required response of the control system is related to the parameters of its adaptive update law

and the impedance controller. The impact of the damping factor of the impedance controller was examined experimentally. It is observed that increase in damping results in slow response but less vibration.

The proposed technique is important in that it has a promising potential for application in biomedical microsurgery. Specifically, it can be applied in cutting delicate tissues with controlled force, thereby preventing tissue damage and improving manipulation stability.

The off-board force determination mechanism presented in this paper relies on magnetic field measurement using Hall-effect sensors. The force model in the paper is developed in a workspace that has a linear relation between the position of the minimum magnetic potential energy point and the Hall-effect sensors' output. For a workspace that has a nonlinear relation, a more complex force model is necessary. The experiment was conducted at room temperature because high-temperature environment affects the linear output of Hall-effect sensors.

The adaptive force tracking algorithm used in this paper is simple and robust enough to control contact with linear and nonlinear stiffness environment. However, when velocity is a key factor to be considered, the algorithm produces force tracking error. Another adaptive law is necessary for this situation.

References

[1] P.-L. Yen and B. L. Davies, "Active constraint control for image-guided robotic surgery," *Proc. Inst. Mech. Eng.*, vol. 224, pp. 623–631, 2010.

[2] S. Kudoh, K. Ogawara, M. Ruchanurucks, and K. Ikeuchi, "Painting robot with multi-fingered hands and stereo vision," *Robot. Auton. Syst.*, vol. 57, no. 3, pp. 279–288, 2009.

[3] A. Lopes and F. Almeida, "A force-impedance controlled industrial robot using an active robotic auxiliary device," *Robot. Comput.-Integr. Manuf.*, vol. 24, no. 3, pp. 299–309, 2008.

[4] Y. Xie, D. Sun, and C. Liu, "A force control approach to a robot-assisted cell microinjection system," *Int. J. Robot. Res.*, vol. 29, no. 9, pp. 1222–1232, 2010.

[5] I. Iordachita *et al.*, "A sub-millimetric, 0.25mN resolution fully integrated fiber-optic force-sensing tool for retinal microsurgery," *Int. J. Comput. Assist. Radiol. Surg.*, vol. 4, pp. 383–390, 2009.

[6] L. M. Capisani and A. Ferrara, "Trajectory planning and second-order sliding mode motion/interaction control for robot manipulators in unknown environment," *IEEE Trans. Ind. Electron.*, vol. 59, no. 8, pp. 3189–3198, Aug. 2012.

[7] G. Duchemin, P. Maillet, P. Poignet, E. Dombre, and F. Pierrot, "A hybrid position/force control approach for identification of deformation models of skin and underlying tissues," *IEEE Trans. Biomed. Eng.*, vol. 52, no. 2, pp. 160–169, Feb. 2005.

[8] N. Hogan, "Impedance control: An approach to manipulation: Part II—Implementation," *J. Dyn. Syst., Meas., Control*, vol. 7, pp. 8–16, 1985.

[9] S. Jung and T. C. Hsia, "Robust neural force control scheme under uncertainties in robot dynamics and unknown environment," *IEEE Trans. Ind. Electron.*, vol. 47, no. 2, pp. 403–412, Apr. 2000.

[10] V. Mallapragada, D. Erol, and N. Sarkar, "A new method of force control for unknown environments," in *Proc. IEEE/RSJ Int. Conf. Intell. Robots Syst.*, 2006, pp. 4509–4514.

[11] L. Huang, S. S. Ge, and T. H. Lee, "An adaptive impedance control scheme for constrained robots," *Int. J. Comput., Syst., Signals*, vol. 5, no. 2, pp. 17–26, 2004.

[12] S. Jung, T. C. Hsia, and R. G. Bonitz, "Force tracking impedance control of robot manipulation under unknown environment," *IEEE Trans. Control Syst. Technol.*, vol. 12, no. 3, pp. 474–483, May 2004.

[13] H. Seraji and R. Colbaugh, "Force tracking in impedance control," *Int. J. Robot. Res.*, vol. 16, no. 1, pp. 97–117, 1997.

[14] H. Wang, K. H. Low, and M. Y. Want, "Reference trajectory generation for force tracking impedance control by using neural network-based environment estimation," in *Proc. IEEE Conf. Robot., Autom. Mechatronics*, 2006, pp. 1–6.

[15] M. B. Khamesee, N. Kato, Y. Nomura, and T. Nakamura, "Design and control of a microrobotic system using magnetic levitation," *IEEE Trans. Mechatronics*, vol. 7, no. 1, pp. 1–14, Mar. 2002.

[16] C. Elbuken, M. B. Khamesee, and M. Yavuz, "Design and implementation of a micromanipulation system using a magnetically levitated MEMS robot," *IEEE Trans. Mechatronics*, vol. 14, no. 4, pp. 434–445, Aug. 2009.

[17] M. P. Kummer, J. J. Abbott, B. E. Kratochvil, R. Borer, A. Sengul, and B. J. Nelson, "OctoMag: An electromagnetic system for 5-DOF wireless micromanipulation," *IEEE Trans. Robot.*, vol. 26, no. 6, pp. 1006–1017, Dec. 2010.

[18] S. Martel *et al.*, "Automatic navigation of an untethered device in the artery of a living animal using a conventional clinical magnetic resonance imaging system," *Appl. Phys. Lett.*, vol. 90, no. 11, 2007, Art. no. 114105.

[19] J. D. J. Gumprecht, T. C. Lueth, and M. B. Khamesee, "Navigation of a robotic capsule endoscope with a novel ultrasound tracking system," *Microsyst. Technol.*, vol. 19, no. 9, pp. 1415–1423, 2013.

[20] M. Mehrtash, X. Zhang, and M. B. Khamesee, "Bilateral magnetic micromanipulation using off-board force sensor," *IEEE/ASME Trans. Mechatronics*, vol. 20, no. 6, pp. 3223–3231, Dec. 2015.

[21] M. Mehrtash, N. Tsuda, and M. B. Khamesee, "Bilateral macro-micro teleoperation using magnetic levitation," *IEEE/ASME Trans. Mechatronics*, vol. 16, no. 3, pp. 459–469, Jun. 2011.

[22] B. Heinrichs, N. Sepehri, and A. B. Thornton-Thrump, "Position-based impedance control of an industrial hydraulic manipulator," *IEEE Control Syst.*, vol. 17, no. 1, pp. 46–52, Feb. 1997.

[23] H. Lim, S. A. Setiawan, and A. Takanishi, "Position-based impedance control of a biped humanoid," *Adv. Robot.*, vol. 18, no. 4, pp. 415–435, 2004.

[24] S. P. Chan and H. C. Liaw, "Generalized impedance control of robot for assembly tasks requiring compliant manipulation," *IEEE Trans. Ind. Electron.*, vol. 43, no. 4, pp. 453–461, Aug. 1996.

[25] Q. Xu, "Precision position/force interaction control of a piezoelectric multimorph microgripper for microassembly," *IEEE Trans. Autom. Sci. Eng.*, vol. 10, no. 3, pp. 503–514, Jul. 2013.

[26] M. Mehrtash and M. B. Khamesee, "Micro-domain force estimation using Hall-effect sensors for a magnetic microrobotic station," *J. Adv. Mech. Des., Syst., Manuf.*, vol. 7, no. 1, pp. 2–14, 2013.

[27] X. Zhang, M. Mehrtash, and M. B. Khamesee, "Dual-axial motion control of a magnetic levitation system using Hall-effect sensors," *IEEE/ASME Trans. Mechatronics*, vol. 21, no. 2, pp. 1129–1139, Apr. 2016.

[28] M. A. L. Mashagbeh, and M. B. Khamesee, "Force control for position interface industrial manipulator working in unknown environment," *Microsyst. Technol.*, vol. 21, no. 12, pp. 2557–2563, 2015.

Xiaodong Zhang received the M.S. degree in electrical engineering from Beijing Jiaotong University, Beijing, China, in 2011. He is currently working toward the Ph.D. degree in mechatronics with the University of Waterloo, Waterloo, ON, Canada.

His research interests include control system design, magnetic levitation, and robotics.

Mir Behrad Khamesee (M'04) received the M.S. and Ph.D. degrees from Mie University, Tsu, Japan, in 1996 and 1999, respectively, both in mechanical engineering (mechatronics) and under a Japanese government scholarship.

He worked in industry in Japan from 1999 to 2002. He was a Postdoctoral Fellow at the University of Alberta, Edmonton, AB, Canada, from 2002 to 2003. In March 2004, he became an Assistant Professor with the University of Waterloo, Waterloo, ON, Canada, and he was promoted two times: in July 2009 to an Associate Professor, and as of July 2015 to the rank of a Professor. His research interests include design, modeling, and control of advanced mechatronics systems, particularly microrobotic magnetic levitation and regenerative electromagnetic shock absorbers.

Dr. Khamesee is involved in conferences program committees, has organized several sessions at international conferences, and is a Technical Reviewer for several IEEE Journals.